Widespread soil bacterium that oxidizes atmospheric methane

Alexander T. Tveit[a,1], Anne Grethe Hestnes[a,1], Serina L. Robinson[a], Arno Schintlmeister[b], Svetlana N. Dedysh[c], Nico Jehmlich[d], Martin von Bergen[d,e], Craig Herbold[b], Michael Wagner[b], Andreas Richter[f], and Mette M. Svenning[a,2]

[a]Department of Arctic and Marine Biology, Faculty of Biosciences, Fisheries and Economics, UiT The Arctic University of Norway, 9037 Tromsoe, Norway; [b]Center of Microbiology and Environmental Systems Science, Division of Microbial Ecology, University of Vienna, 1090 Vienna, Austria; [c]Winogradsky Institute of Microbiology, Research Center of Biotechnology of Russian Academy of Sciences, 117312 Moscow, Russia; [d]Department of Molecular Systems Biology, Helmholtz Centre for Environmental Research-UFZ, 04318 Leipzig, Germany; [e]Faculty of Life Sciences, Institute of Biochemistry, University of Leipzig, 04109 Leipzig, Germany; and [f]Center of Microbiology and Environmental Systems Science, Division of Terrestrial Ecosystem Research, University of Vienna, 1090 Vienna, Austria

Edited by Mary E. Lidstrom, University of Washington, Seattle, WA, and approved March 7, 2019 (received for review October 22, 2018)

The global atmospheric level of methane (CH_4), the second most important greenhouse gas, is currently increasing by ∼10 million tons per year. Microbial oxidation in unsaturated soils is the only known biological process that removes CH_4 from the atmosphere, but so far, bacteria that can grow on atmospheric CH_4 have eluded all cultivation efforts. In this study, we have isolated a pure culture of a bacterium, strain MG08 that grows on air at atmospheric concentrations of CH_4 [1.86 parts per million volume (p.p.m.v.)]. This organism, named *Methylocapsa gorgona*, is globally distributed in soils and closely related to uncultured members of the upland soil cluster α. CH_4 oxidation experiments and ^{13}C-single cell isotope analyses demonstrated that it oxidizes atmospheric CH_4 aerobically and assimilates carbon from both CH_4 and CO_2. Its estimated specific affinity for CH_4 (a^0_s) is the highest for any cultivated methanotroph. However, growth on ambient air was also confirmed for *Methylocapsa acidiphila* and *Methylocapsa aurea*, close relatives with a lower specific affinity for CH_4, suggesting that the ability to utilize atmospheric CH_4 for growth is more widespread than previously believed. The closed genome of *M. gorgona* MG08 encodes a single particulate methane monooxygenase, the serine cycle for assimilation of carbon from CH_4 and CO_2, and CO_2 fixation via the recently postulated reductive glycine pathway. It also fixes dinitrogen and expresses the genes for a high-affinity hydrogenase and carbon monoxide dehydrogenase, suggesting that atmospheric CH_4 oxidizers harvest additional energy from oxidation of the atmospheric trace gases carbon monoxide (0.2 p.p.m.v.) and hydrogen (0.5 p.p.m.v.).

methane | USC alpha | trace gases | isolate | filter cultivation

The atmospheric concentration of methane (CH_4), a potent greenhouse gas and a precursor for tropospheric ozone pollution (1), has increased from 0.720 to over 1.86 p.p.m.v. since the beginning of the industrial era (2–4). The primary sinks of atmospheric CH_4 are abiotic oxidation by tropospheric hydroxyl radicals and the activity of aerobic methane oxidizing bacteria (MOB) in unsaturated soils (5–7). MOB belong to a small number of bacterial lineages within the Gamma- and Alphaproteobacteria as well as the Verrucomicrobia (8, 9). A defining characteristic of these bacteria is the use of methane monooxygenase (MMO), the unique multicomponent enzyme system catalyzing an initial oxidative attack on CH_4 (9, 10). The first MOB was described in 1906 (11) but it was not until the early 1990s that cultivation-independent indications of the existence of MOB that live on atmospheric CH_4 concentrations (atmMOB) were obtained (12–15). Interestingly however, calculations indicated that atmospheric CH_4 does not supply the maintenance energy requirements of cultivated methanotrophs (6), suggesting either that atmMOB are energetically more efficient, have a higher affinity or specific affinity (a^0_s) for CH_4, or use additional energy sources. Labeling experiments combined with phylogenetic marker analyses demonstrated that these atmMOB constituted two as-yet-uncultured clades within the Alpha- and Gammaproteobacteria (16–18) which were designated as upland soil clusters α and γ (USCα and USCγ, respectively). Interest in soil atmMOB has increased significantly since then because they are responsible for the only known biological removal of atmospheric CH_4 (2, 6) and thus play a key role in the atmospheric CH_4 budget. Importantly, atmMOB appear to be very sensitive to many types of anthropogenic disturbance, including conversion of forests to agriculture, fertilization, acidification, and nitrogen deposition. Thus, efforts to manage this biological CH_4 sink could be more effective if we knew more about the biology of the microorganisms responsible for it (6).

Recent research has revealed that not only members of the USCs can oxidize atmospheric CH_4 since this metabolic capability was also reported for members of the well-known MOB genera *Methylocystis* and *Methylosinus* (19–23). In addition to the "conventional," low-affinity particulate MMO, these bacteria possess a high-affinity form of this enzyme, which is responsible for oxidizing CH_4 at low partial pressures (19). Importantly however, these

Significance

Increasing atmospheric methane concentrations contribute significantly to global warming. The only known biological sink for atmospheric methane is oxidation by methane oxidizing bacteria (MOB). Due to the lack of pure cultures, the physiology and metabolic potential of MOB that oxidize atmospheric methane remains a mystery. Here, we report on isolation and characterization of a MOB that can grow on air and utilizes methane at its atmospheric trace concentration as a carbon and energy source. Furthermore, this strain has the potential to utilize five additional atmospheric gases, carbon dioxide, carbon monoxide, hydrogen, nitrogen, and oxygen to supply its metabolism. This metabolic versatility might be the key to life on air and this discovery is essential for studying the biological methane sink.

Author contributions: A.T.T., A.G.H., S.L.R., A.S., M.W., A.R., and M.M.S. designed research; A.T.T., A.G.H., S.L.R., A.S., N.J., M.v.B., C.H., and M.M.S. performed research; A.T.T., A.G.H., S.L.R., A.S., S.N.D., N.J., M.v.B., C.H., M.W., A.R., and M.M.S. analyzed data; and A.T.T., S.L.R., S.N.D., C.H., M.W., A.R., and M.M.S. wrote the paper.

The authors declare no conflict of interest.

This article is a PNAS Direct Submission.

Data deposition: The sequences reported in this paper have been deposited in the GenBank database (accession no. CP024846).

[1]A.T.T. and A.G.H. contributed equally to this work.

[2]To whom correspondence should be addressed. Email: mette.svenning@uit.no.

This article contains supporting information online at www.pnas.org/lookup/suppl/doi:10.1073/pnas.1817812116/-/DCSupplemental.

Published online April 8, 2019.

MOB were not shown to grow at atmospheric CH_4 concentrations and likely rely on storage compounds during periods of low CH_4 availability that are built up during periodic exposures to high concentrations of CH_4 (6, 24).

Research on USC clades spans nearly two decades. As no cultured representatives are available and even their 16S rRNA genes remained unknown until very recently (25), these bacteria could be traced in the environment only by using the gene encoding a subunit of the particulate methane monooxygenase (*pmoA*) as a specific marker (16, 18, 24, 26, 27). As revealed in *pmoA*-based studies, USCs occur exclusively in soils, with USCα being found primarily at pH neutral and acidic conditions, while USCγ is thriving mostly in pH neutral and alkaline soils (8, 16). Notably, both groups have also been observed in arctic upland soils (28). During the last years, information on their distribution, abundance, and activity was supplemented with first insights into their genomic repertoire as obtained from metagenomics (25, 29–31), but no complete genome sequence of a USC member has yet been reported.

In this study, we report the isolation of a pure culture of a member of the USCα clade, strain MG08, the basic morphological and physiological traits of this bacterium, and its complete genome sequence. Microcolony-growth experiments on floating filters revealed that our isolate grows on polycarbonate and inorganic filters floating on nitrate mineral salt medium (NMS) under an atmosphere of ambient air. Combined genomic and proteomic analyses revealed that the cultured USCα strain encodes and expresses an enzymatic repertoire for using CH_4, carbon monoxide, and hydrogen, suggesting that the latter two trace gases provide additional energy sources. We explicitly showed oxidation of atmopsheric CH_4 by *Methylocapsa gorgona* MG08 and estimated that it has a much higher specific affinity (a^0_s) for CH_4 than other available MOB isolates (23). However, cultivation of other MOB on floating filters under an atmosphere of ambient air showed that strains with a lower specific affinity (a^0_s) for CH_4 were also able to grow, questioning whether a "high affinity" or "high-specific affinity" for CH_4 is the decisive prerequisite for an oligotrophic life on air.

Results and Discussion

After 2 y of enrichment a pure culture of a MOB from a landfill soil inoculum was obtained. The complete genome sequence of strain MG08 was determined from 94,080 long reads (Pacific Biosciences) which assembled into a single circular chromosome with 3,326,440 bp and a GC content of 58.94% (*SI Appendix*, Table S2). All reads mapped to the genome confirming that no contaminating organisms were present in the culture. The genome encoded 46 tRNA genes, a single 16S, 23S, and 5S rRNA gene operon, a single *pmoCAB* operon, and one orphan *pmoC* gene.

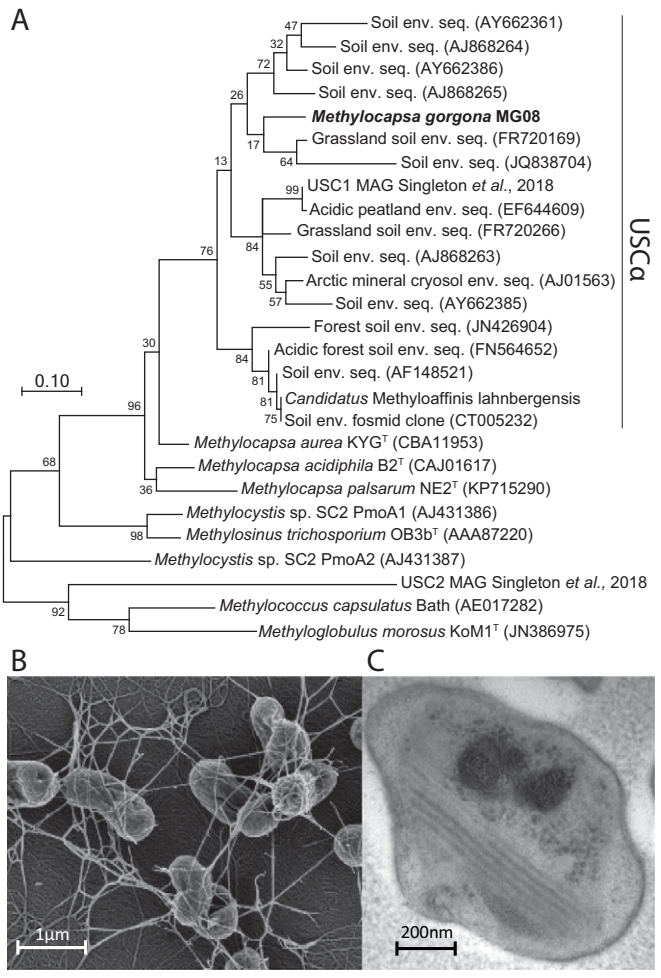

Fig. 1. Phylogenetic relationship of the PmoA and electron micrographs of *M. gorgona* MG08. (*A*) The unrooted maximum-likelihood tree based on 155-aa positions was computed using the Jones Taylor Thornton matrix-based model of amino acid substitution. Env. Seq., environmental sequence (clone or DGGE sequence). The PmoA of *M. gorgona* MG08 clusters with other uncultured MOB within the USCα JR1/cluster 5 (*Methylocella* species does not carry the genes that encode pMMO and is therefore not represented in the tree). Bootstrap values are presented at branch points (1,000 data resamplings). Bar, 0.05-aa substitutions per site. (*B*) Scanning electron micrograph of *M. gorgona* MG08 cells grown at 21 °C in liquid culture with 20% CH_4 headspace without shaking. (*C*) Transmission electron micrograph of cells grown under the same conditions showing intracytoplasmic membranes of type III and inclusions that resemble PHB granules.

Phylogeny and Global Distribution. The inferred PmoA sequence of the newly cultured MOB grouped within the previously described USCα Jasper Ridge 1/cluster 5 (32) (Fig. 1*A*) and had up to 87.7% amino acid identity with environmentally retrieved sequences (FR720169) within this cluster. Consistently, 16S rRNA gene-based phylogenetic analyses showed that this MOB clusters with the 16S rRNA gene sequence (97.8% identity) of the uncultured USCα *Candidatus* Methyloaffinis lahnbergensis (25) (*SI Appendix*, Fig. S1). Two additional USCα genomes that were recently assembled from subarctic mire metagenomes did not contain 16S rRNA genes (31). The average amino acid identity (AAI) between our isolate and previously published USCα metagenome-assembled genomes (MAGs) ranges from 70% to 72% (Fig. 2*A*) confirming that our isolate and existing USCα MAGs likely belong to the same genus. Interestingly, the AAI between our isolate and characterized *Methylocapsa* species ranges from 67% to 69%. This is comparable to the AAI shared within validly published *Methylocapsa* species (67–72%), suggesting that our isolate and, by extension, other USCα MAGs are all members of the genus *Methylocapsa*. Genomic average nucleotide identity (gANI) shared between our isolate and other members of the *Methylocapsa* genus, including the USCα MAGs, ranges from 74% to 79%, demonstrating that the isolate constitutes a species within the genus *Methylocapsa* (Fig. 2*A*), which we named *M. gorgona* MG08; gor.go'na. L. fem. n. *gorgona* (from Gr. fem. n. *gorgonè*) a vicious female monster from Greek mythology with sharp fangs and hair of living, venomous snakes in reference to the hair-like structures produced by the type of strain (Fig. 1*B*).

The identification of *M. gorgona* as a member of the USCα group was confirmed by phylogenetic analysis based on a concatenated alignment of 34 conserved taxonomic marker genes (Fig. 2*B*). However, we did not recover strong support for a monophyletic clade of *Methylocapsa*, regardless of whether we considered USCα as part of the genus or not. This lack of resolution was due to the inclusion of two strains of *Methylocella*

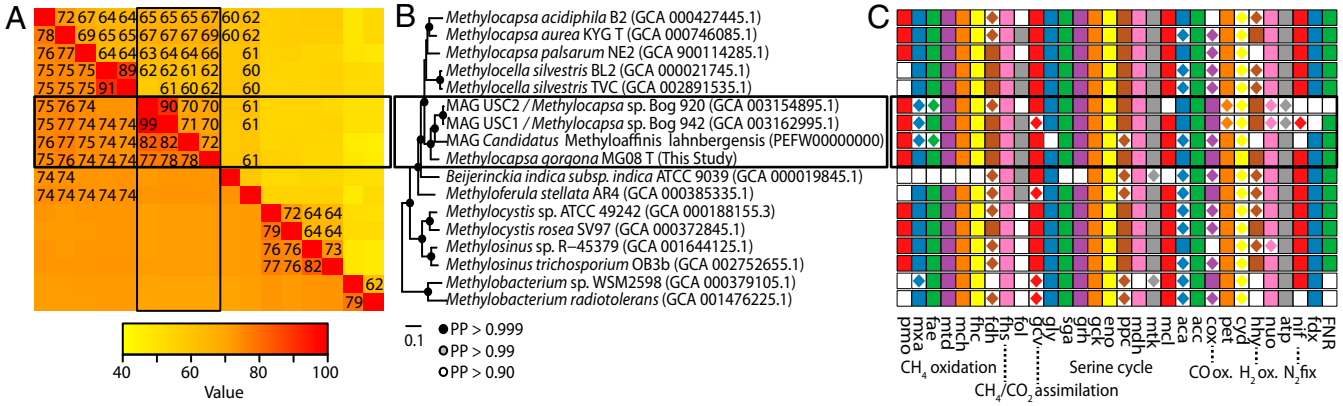

Fig. 2. Average nucleotide and amino acid identities, phylogenetic relationship, and central metabolism comparison between *M. gorgona* MG08 and its genome sequenced relatives. (*A*) Symmetrical matrix of pairwise gANI and AAIs between all strains and MAGs and ordered as in *B*. ANI is presented in the *Lower Left* triangle and values ≥74 are provided. AAI is presented in the *Upper Right* triangle and values ≥60 are provided. *M. gorgona* MG08 and *Ca.* M. lahnbergensis (AAI, 71.3; ANI, 78.1), MAG USC1 (AAI, 70.1; ANI, 78.0), MAG USC2 (AAI, 70.0; ANI, 77.3), *M. aurea KYG T* (AAI, 69.3; ANI, 72.5), *M. acidiphila B2* (AAI, 67.4; ANI, 74.75), *M. palsarum NE2* (AAI, 66.1; ANI, 67.9) and *M. silvestris BL2* (AAI, 62.5; ANI, 69.9) are below the species threshold of 96.6 ANI (3) and 95 AAI (4). (*B*) The phylogenomic tree was calculated with 10 independent chains of 11,000 generations under the LG model with four rate categories, using an input alignment of 34 concatenated marker genes (*Materials and Methods*). A total of 6,000 generations of each chain were discarded as burn-in, the remainder were subsampled every five trees (bpcomp -x 6000 5 11000) and pooled together for calculation of the reported 50% consensus tree and bipartition posterior probabilities (maxdiff = 0.814, meandiff = 0.010076). The model and number of rate categories was identified using ModelFinder (*Materials and Methods*). (*C*) Distribution of functional complexes presented in Fig. 4 and *SI Appendix*, Table S1 were determined using blast (5), OrthoFinder (6), and manual examination of trees. Presence of a complete complex is indicated by a solid square. Complexes that are incomplete are indicated with an embedded diamond. Abbreviations for functional complexes: aca, carbonic anhydrase; acc, acetyl-CoA carboxylase; atp, ATP synthase; cox, carbon monoxide dehydrogenase; cyd, terminal cytochrome oxidase; eno, enolase; fae, formaldehyde activating enzyme; fdh, formate dehydrogenase; fdx, ferredoxin, 2Fe-2S; fhc, formyltransferase/hydrolase complex; fhs, formate–tetrahydrofolateligase; FNR, ferredoxin-NADP+ oxidoreductase; fol, bifunctional 5,10-methylene-tetrahydrofolatedehydrogenase, and 5,10-methylene-tetrahydrofolatecyclohydrolase; gck, 2-glycerate kinase; gcv, glycine cleavage complex; gly, serine hydroxymethyltransferase; hhy, [NiFe] hydrogenase; hpr, hydroxypyruvate reductase; mch, methenyl tetrahydromethanopterin cyclohydrolase; mcl, malyl-CoA lyase; mdh, malate dehydrogenase; mtd, NAD(P)-dependent methylene tetrahydromethanopterin dehydrogenase; mtk, malate thiokinase; mxa, methanol dehydrogenase; nif, nitrogenase; nuo, NADH-quinone oxidoreductase; pet, ubiquinol-cytochrome *c* reductase; pmo, particulate methane monooxygenase; ppc, phosphoenolpyruvate carboxylase; and sga, serine–glyoxylate aminotransferase.

silvestris in our phylogenetic reconstruction. These strains share 64–65% AAI with recognized species of *Methylocapsa*, which is lower than the 67–72% AAI shared within recognized *Methylocapsa* but similar to the 63–69% AAI shared between recognized species of *Methylocapsa* and USCα genomes (Fig. 2*A*). Together, *Methylocapsa*, USCα, and *Methylocella* all form a single strongly supported clade. Although AAI values and phylogenetic arguments taken together support the assignment of *M. gorgona* MG08 and other USCα as members of the *Methyolcapsa*, our data do not resolve the relationship between *Methylocella* and lineages of *Methylocapsa*. We hope that the isolation and genome sequencing of additional *Methylocapsa* strains in the future will help resolve the branching order and relationships within this clade.

Screening of all publicly available environmental 16S rRNA gene amplicon datasets identified 194,764 sequences in 1,537 datasets (0.8% of all screened datasets) that were identical or very similar (>97% identity) to the 16S rRNA gene of *M. gorgona* MG08. These datasets originated almost exclusively from terrestrial environments (primarily from soil) spanning six continents, with latitudes ranging from the high arctic Svalbard over the tropics to southern Australia and New Zealand (Fig. 3), demonstrating that microbes identical to or highly related to our isolate are globally distributed in terrestrial ecosystems.

Comparative Genomics and Proteomics. The genome of *M. gorgona* MG08 encodes and expresses several pathways that are typically found in alphaproteobacterial MOB, but excitingly also contains unique metabolic features (Figs. 2*C* and 4 and *SI Appendix*, Table S1). Like other MOB it uses a particulate methane monooxygenase (pMMO) for CH_4 oxidation to methanol. pMMO requires copper, but the methanobactin (a copper-binding peptide) operon found in various *Methylocystis* species (33) is not present in the genome of *M. gorgona* MG08. However, we detected a homolog to one member of this operon, the methanobactin biosynthesis cassette protein MbnB/DUF692 (PF05114.12). In *M. gorgona* MG08 and other *Methylocapsa* species, this gene is part of a conserved gene cluster of four genes homologous to the GIG operon in *Legionella pneumophila* which responds to altered copper concentrations (34). These genes encode a putative integral membrane signal protein (DUF2282–PF10048.8, expression confirmed in proteome in the presence of 1 μM Cu), a putative DNA binding protein (DUF2063–PF09836.8), and an inner membrane protein (DoxX domain containing PF07681). We observed a PQQ-linked methanol dehydrogenase (MxaFJGI)

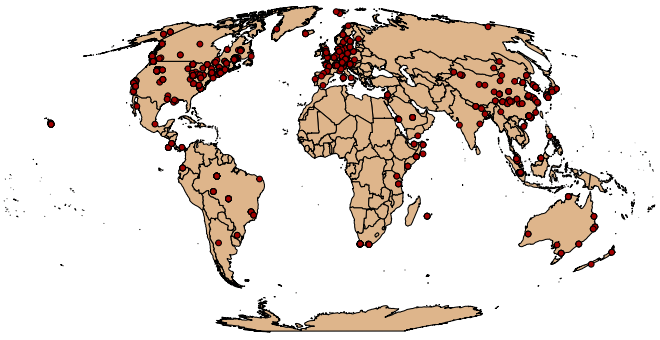

Fig. 3. Global distribution of the *M. gorgona* lineage. The map indicates sampling locations of public SRA datasets containing members of the *M. gorgona* lineage (*Materials and Methods*). The *M. gorgona* lineage was identified in 1,537 SRA datasets, of which 1,240 are shown. Latitude and longitude were unavailable for the remaining 297 datasets.

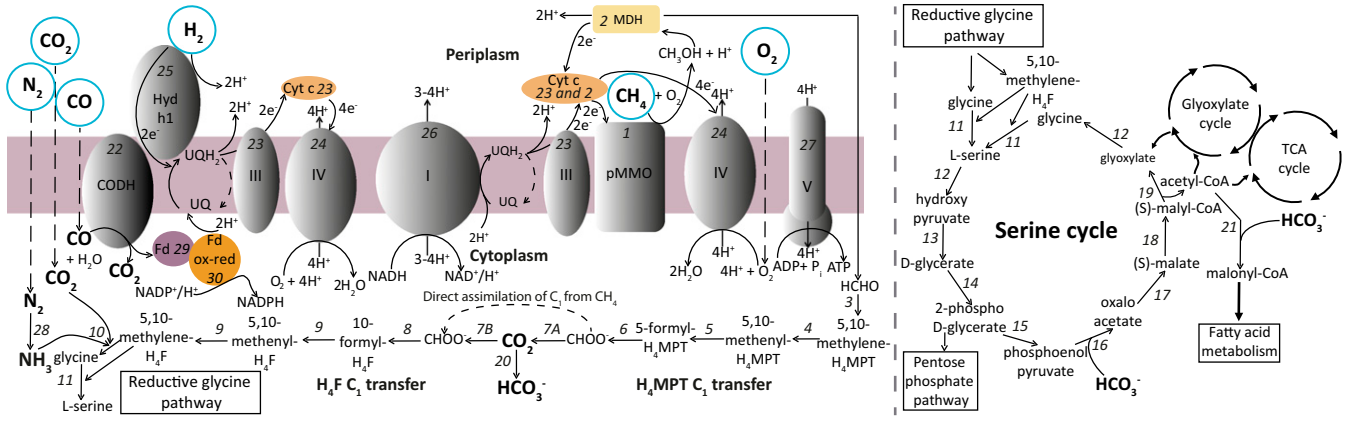

Fig. 4. The central carbon and energy metabolism of *M. gorgona* MG08 as predicted from its genome and confirmed by proteomics. H_4MPT, tetrahydromethanopterin. Dashed black arrows indicate passive diffusion across the cell membrane. Numbers for the metabolic steps in the figure refer to the following enzyme names: (1) particulate methane monooxygenase, (2) methanol dehydrogenase and corresponding cytochrome *c*, (3) formaldehyde activating enzyme, (4) NAD(P)-dependent methylene tetrahydromethanopterin dehydrogenase, (5) methenyl tetrahydromethanopterin cyclohydrolase, (6) formyltransferase/hydrolase, (7A) NAD-dependent formate dehydrogenase, (7B) molybdopterin binding reversible formate dehydrogenase/CO_2 reductase, (8) formate-tetrahydrofolate ligase, (9) bifunctional 5,10-methylene-tetrahydrofolate dehydrogenase and 5,10-methylene-tetrahydrofolate cyclohydrolase, (10) glycine cleavage system, (11) serine hydroxymethyltransferase, (12) serine–glyoxylate aminotransferase, (13) hydroxypyruvate reductase, (14) 2-glycerate kinase, (15) enolase, (16) phosphoenolpyruvate carboxylase, (17) malate dehydrogenase, (18) malate thiokinase, (19) malyl-CoA lyase, (20) carbonic anhydrase, (21) acetyl-CoA carboxylase, (22) [MuCo] class I carbon monoxide dehydrogenase, (23) cytochrome *c* reductase and corresponding cytochrome *c*, (24) cytochrome *c*/d/o terminal oxidases (cytochrome d oxidase—*cydAB*, cytochrome o ubiquinol oxidase—*cyoABCD*, heme-copper cytochrome *c* oxidase type A1 – *ctaAEGBC*, heme-copper cytochrome type C cbb_3 oxidase—*ccoNOQP* and heme-copper cytochrome *c* oxidase type A1—*coxCAB*). (25) [NiFe] group 1h hydrogenase, (26) NADH dehydrogenase, (27) ATP synthase, (28) nitrogenase, (29) ferredoxin, 2Fe-2S, and (30) ferredoxin-$NADP^+$ oxidoreductase. All enzymes and electron carrier proteins were also detected in the proteome, with the exception of the nitrogenase and the cbb_3 oxidase. A full list of the proteins, corresponding genes, and genome entries are found in *SI Appendix*, Table S1.

which uses calcium as a catalytic cofactor to convert methanol to formaldehyde which is absent in the closely related USCα MAGs (Datasets S1 and S2). Additionally, a lanthanide-dependent methanol dehydrogenase of the *xoxF* family 5 with an amino acid identity of 75% to *Methylobacterium nodulans* ORS 2060 and 72% to *Methylobacterium extorquens* CM4 (35), for which lanthanide-dependent regulation of methylotrophy was thoroughly investigated (36), is encoded in the genome. In liquid culture with 20% CH_4 (vol/vol) in the headspace and no addition of lanthanides, the expression of *mxaF* in *M. gorgona* MG08 was approximately 10 times higher than that of *xoxF* (*SI Appendix*, Table S1). *M. gorgona* MG08 encodes a complete pathway for tetrahydromethanopterin (H_4MPT)-mediated formaldehyde oxidation to formate, a nonreversible formate dehydrogenase for NADH generating formate oxidation to CO_2, and the pathway for C_1 incorporation in the serine cycle via tetrahydrofolate (H_4F)-mediated C_1 transfer (Fig. 4). A putative pathway of formaldehyde oxidation to formate via H_4F also exists. This pathway requires spontaneous conversion of formaldehyde to 5,10-methylene H_4F for its operation (37). However, based on previous experiments with *M. extorquens*, where both pathways are present but only the H_4MPT pathway is responsible for formaldehyde oxidation (38), we consider it unlikely that the H_4F pathway is responsible for formaldehyde oxidation in *M. gorgona* MG08. We also identified gene sets for a complete oxidative tricarboxylic acid cycle (TCA), the Entner–Doudoroff pathway, the pentose phosphate pathway, and the glyoxylate cycle, as well as a complete respiratory chain with five versions of terminal respiratory oxidases, indicating that it has the ability to grow under different oxygen concentrations (Fig. 4 and *SI Appendix*, Table S1). However, the genome did not encode a complete ethylomalonyl-CoA pathway. *M. gorgona* MG08 has an incomplete Calvin–Benson–Bassham (CBB) cycle and therefore contrasts in this respect with other members of *Methylocapsa*, *Methylocella*, and some gammaproteobacterial and verrucomicrobial MOB (39–44). Its single RuBisCO gene homolog encodes a type IV RuBisCO that does not allow CO_2 fixation (*SI Appendix*, Fig. S2*A*) but instead may be involved in methionine metabolism, oxidative stress response, or sulfur oxidation (45). This suggests that *M. gorgona* MG08 has lost the gene for the canonical RuBisCO. This is not a general feature in USCs as the USC1 and USC2 MAG (31) encoded both the canonical RuBisCO and a type IV RuBisCO, while the genes for the canonical RuBisCO and its type IV homolog were not found in the incomplete genome of *Ca.* M. lahnbergensis (25). Further insights into the distribution of the canonical RuBisCO must await the complete genome sequence of *Ca.* M. lahnbergensis and other USC strains. *M. gorgona* MG08 does have a complete reductive glycine pathway for CO_2 fixation (46) which includes a formate dehydrogenase complex homologous with the oxygen-tolerant complex in *Rhodobacter capsulatus* that was experimentally confirmed to catalyze CO_2 reduction (*SI Appendix*, Fig. S2*B*) (47). This pathway overlaps with the H_4F-mediated C_1 transfer for simultaneous assimilation of CO_2 and ammonia (NH_3). Genes for this pathway were consistently found in all genomes of the genera *Methylocapsa*, *Methylocella*, and the three USCα MAGs, but of the three MAGs only *Ca.* M. lahnbergensis contained all necessary genes for the complete pathway (Dataset S1). In addition, *M. gorgona* MG08 possesses the complete *nifHDKENX* operon that codes for structural nitrogenase components, which, with the exception of the single gene *nifH* in USC1 is absent from the draft MAG of *Ca.* M. lahnbergensis USC1 and USC2 (Fig. 2*C* and Dataset S1). NifH and NifD phylogenies showed that the *nif* genes of *M. gorgona* MG08 have a different evolutionary origin than those of other closely related cultures (*SI Appendix*, Fig. S3). Genes encoding hydroxylamine oxidoreductase (*hao*) and cytochrome c_{554} were absent from the genome, confirming that *M. gorgona* MG08 does not have the potential to derive energy from ammonia oxidation (48). Interestingly, *M. gorgona* MG08 contains genes that encode an O_2-tolerant/insensitive [NiFe] group 1h high-affinity respiratory hydrogenase (*hhyL* and *hhyS*) and a [MoCu] class I respiratory carbon monoxide dehydrogenase (Fig. 2*C* and *SI Appendix*, Fig. S4). As these enzymes belong to the same lineages as those encoded by nonmethanotrophic communities in Antarctic desert soils (49) and the soil actinobacterium *Mycobacterium smegmatis* (50) that are capable of using atmospheric concentrations of H_2 and CO, *M. gorgona* MG08 might

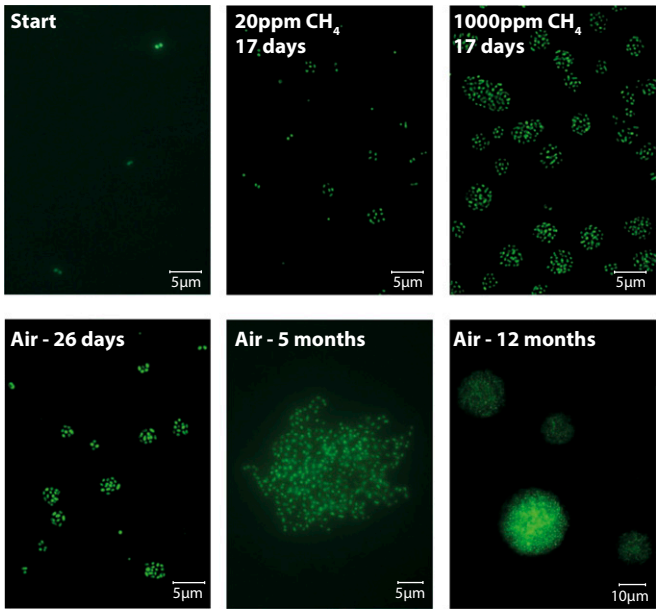

Fig. 5. Microcolonies of *M. gorgona* MG08 cultivated at different CH_4 concentrations. Microcolonies were grown on polycarbonate filters floating on liquid nitrate mineral salt medium for the number of days specified on each picture, either in closed jars with air amended with different concentrations of CH_4, or exposed to unamended air. For fixation, the filters were transferred to fresh-made 2% paraformaldehyde in 1× PBS in the refrigerator overnight. For staining, filters were transferred (side with bacteria up) on top of 200 μL droplets of 1,000× SYBRgreen and incubated for 10 min, washed, and air dried.

be able to conserve energy from aerobic respiration of these trace gases at atmospheric concentrations as well. This feature is obviously more widespread among USCα members as the draft genomes of *Ca.* M. lahnbergensis, USC1 and USC2 also encode closely related CO dehydrogenases (Fig. 2*C* and *SI Appendix*, Fig. S4*B*), and USC1 and USC2 (the incomplete genome of *Ca.* M. lahnbergensis lacks a high-affinity hydrogenase) contain hydrogenase genes that are highly similar to the one found in *M. gorgona* MG08 (Fig. 2*C* and *SI Appendix*, Fig. S4*A*).

Proteomic analyses of *M. gorgona* MG08 grown in liquid culture under an atmosphere containing 20% CH_4 (but at ambient concentrations of CO and H_2) in the presence of 10 mM nitrate confirmed that all proteins shown in Fig. 4 except nitrogenase and a cbb3 type cytochrome *c* oxidase were expressed (*SI Appendix*, Table S1). Among the detected proteins were those of the reductive glycine pathway, including its CO_2 reductase, the high-affinity hydrogenase, and carbon monoxide dehydrogenase.

Physiology and Morphology. *M. gorgona* MG08 phylogenetically belongs to the clade of putative high-affinity alphaproteobacterial USCα MOB. We therefore performed experiments to test whether this isolate can grow on ambient air containing an atmospheric CH_4 concentration using a microcolony cultivation technique of filters floating on liquid nitrate mineral salt medium without any added energy or carbon source. These experiments unequivocally demonstrated that *M. gorgona* MG08 grew in ambient air (~1.86 p.p.m.v. CH_4, ~0.2 p.p.m.v. CO, and ~0.5 p.p.m.v. H_2) and higher (20 and 1,000 p.p.m.v.) CH_4 concentrations (Fig. 5). After up to 3 wk of incubation the largest colonies were observed under 1,000 p.p.m.v. CH_4 while smaller colonies formed under 20 p.p.m.v., similar to those in unamended atmospheric air, confirming that increased concentrations of CH_4 stimulated growth. Continued growth of *M. gorgona* MG08 in unamended air was confirmed after 5 and 12 mo (Fig. 5), reaching more than 10 times its initial population size after 5 mo and continuing to grow and form spherical colonies observable after 12 mo (Fig. 5). In comparison, starving *Sinorhizobium meliloti* were able to triple their initial population size using intracellular polyhydroxybutyrate (PHB) as a carbon and energy source and maintain its population for 5 mo before it declined to a level below its initial size (51). A species more closely related to *M. gorgona* MG08, the MOB *Methylocystis parvus* OBBP, did not replicate at all using stored PHB and depended on the access to CH_4 for co-oxidation of the two substrates for growth (52). Considering this, we find it implausible that *M. gorgona* MG08 would depend entirely upon PHB for its growth over the course of 12 mo, but it is possible that any existing PHB storages were tapped during the incubation period and used as a carbon and energy supplement to its main diet.

M. gorgona MG08 encodes only a single copy of the particulate methane monooxygenase which was also detected in its proteome. This shows that the same enzyme is responsible for catalyzing CH_4 oxidation at both high and low CH_4 concentrations. To confirm that *M. gorgona* MG08 is able to oxidize atmospheric concentrations of CH_4 we performed a CH_4 oxidation and microcolony-growth experiment with cells on floating filters under atmopheric air (1.86 p.p.m.v. CH_4). The results clearly show that CH_4 was oxidized during the 120 d of incubation under atmospheric air (Fig. 6*A*). Inspection of the filters confirmed cell growth (Fig. 6*B*). *M. gorgona* MG08 also carries single copies of the high-affinity respiratory hydrogenase and carbon monoxide dehydrogenase and both were expressed under 20% CH_4 headspace concentrations, without added CO or H_2. Thus, it seems likely that these proteins are constitutively expressed at different CH_4 concentrations and thus contribute to the energy harvest from air. However, it is not possible to conclude on this matter until we have successfully determined the proteome of *M. gorgona* MG08 grown on air, which was not yet achieved due to biomass limitations. Furthermore, due to the difficulty in preparing headspace atmospheres and media free of trace amounts of

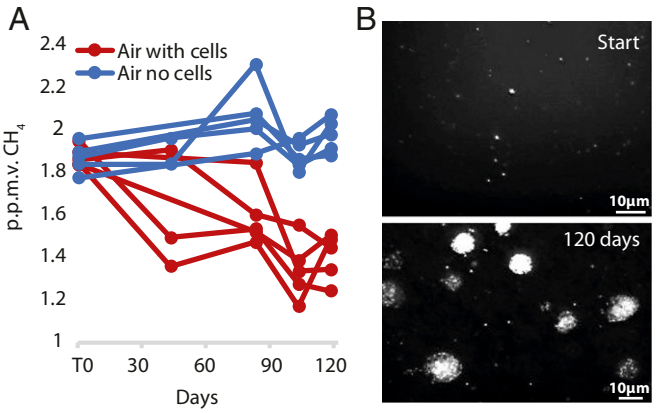

Fig. 6. CH_4 oxidation by *M. gorgona* MG08 microcolonies incubated on floating filters under atmospheric air (*A*). Microcolony formation under atmospheric air (*B*). (*A*) Five 170-mL bottles with floating polycarbonate filters were incubated on 35 mL 1/10 diluted nitrate mineral salt media (*Materials and Methods*) under atmospheric air (135 mL 1 atm headspace, sealed with rubber stopper) for 120 d. An additional set of five bottles was incubated without filters as a negative control for CH_4 oxidation. A two-sample *t* test assuming equal variances confirmed that headspace CH_4 concentrations were significantly different in bottles with filters containing cells (*P* value < 0.001), compared with those without cells. (*B*) Filters from *A* were manually inspected to identify colony formation. (*Top*) Showing single cells before incubation. (*Bottom*) Colonies formed after 120-d incubation in one of the bottles from *A*. For staining in *B*, filters were transferred (side with bacteria up) on top of 200 μL droplets of 1,000× SYBRgreen and incubated for 10 min, washed, and air dried.

alternative carbon and energy sources such as CO (0.2 p.p.m.v. in air) and H_2 (0.5 p.p.m.v. in air), and EDTA (53) (1.1 μM in the 1/10 diluted nitrate mineral salt medium used), respectively, we cannot yet conclude whether growth is possible solely on atmospheric CH_4. However, growth did occur on high-purity carbon-free alumina matrix Anodisc inorganic filters floating on nitrate mineral salt medium under atmospheric air (*SI Appendix*, Fig. S5). This confirms that the cells at least did not depend on bisphenyl A (BPA) leaking from the polycarbonate filters (54, 55) as an additional carbon and energy source.

An additional CH_4 oxidation experiment, using cells in liquid culture under a range of CH_4 concentrations, was performed to estimate the half saturation constant [$K_{m(app)}$] for *M. gorgona* MG08 (*SI Appendix*, Fig. S6). We show that it has a $K_{m(app)}$ of 4.905 μM, similar to that observed for *Methylocapsa acidiphila* B2, *M. parvus*, *Methylocystis* sp. SC2, and many other MOB strains (23). In contrast to *M. gorgona* MG08, neither of these strains was previously found to grow at atmopheric CH_4 concentrations. The specific affinity [$a^0_s = V_{max(app)}/K_{m(app)}$] was suggested as a better measure for oligotrophy (6) as *Methylocystis* sp. LR1 displayed high-affinity activity (K_m of ∼100 nM) at low CH_4 concentrations (<275 p.p.m.v.) and low-affinity activity (K_m of ∼1 μM) when CH_4 concentrations were higher while its specific affinity remained constant (56). With a $V_{max(app)}$ of 9.54×10^{-10} μmol·cell^{-1}·h^{-1}, the specific affinity of *M. gorgona* MG08 is ∼195 ($\times 10^{-12}$ L·cell^{-1}·h^{-1}), which is ∼17 times higher than the corresponding value of *M. acidiphila* B2 (12×10^{-12} L·cell^{-1}·h^{-1}), ∼10 times higher than for *Methylocystis* sp. LR1 (20×10^{-12} L·cell^{-1}·h^{-1}), and ∼6 times higher than for *Methylocystis* sp. SC2 (34×10^{-12} L·cell^{-1}·h^{-1}), formerly the MOB with the highest known a^0_s (23). The high-affinity MOB is thus probably better defined as a high-specific affinity MOB as suggested by Dunfield (6) more than 10 y ago, but a confirmation of this must await standardized comparisons between USCα and other MOB strains.

Despite having lower specific affinities (a^0_s) than *M. gorgona* MG08, we decided to test whether other *Methylocapsa* species are able to grow at atmospheric CH_4 concentrations. Surprisingly, both *M. acidiphila* and *Methylocapsa aurea* were able to also grow on floating filters incubated under atmospheric air (*SI Appendix*, Fig. S7). This suggests that the ability of MOB to grow on filters floating on nitrate mineral salt medium under unamended air is not a unique capability of species within the USCα, and not dependent on a high a^0_s for CH_4. However, the apparent success of USCα in many upland soils may still be a result of having the highest a^0_s.

Consistent with the physiological and genomic predictions, NanoSIMS experiments performed on microcolonies on polycarbonate filters qualitatively showed that *M. gorgona* MG08 incorporated ^{13}C-labeled carbon into its biomass when grown in a closed jar containing 20 p.p.m.v. $^{13}CH_4$ and unlabeled CO_2 (Fig. 7*A*). Incorporation of ^{13}C was also observed in the presence of $^{13}CO_2$ at 20 p.p.m.v. and unlabeled CH_4 (Fig. 7*B*), as expected from CO_2/HCO_3^- incorporation via the carboxylation reaction of the serine cycle (enzyme no. 16, Fig. 4). There is also the possibility that CO_2 could be assimilated via the reductive glycine pathway, but with the current data the different possible entry points of carbon assimilated from CO_2 cannot be distinguished. Accumulation of $^{13}CO_2$ in the headspace of the cultures during incubation with 20 p.p.m.v. and 1,000 p.p.m.v. $^{13}CH_4$ confirmed that the organism is able to oxidize CH_4 completely to CO_2 and subsequently release CO_2 from the cell (*SI Appendix*, Fig. S8).

Additional physiological characterizations of *M. gorgona* MG08 were carried out in liquid cultures grown at a high CH_4 concentration. Efficient growth was observed when N_2 was offered as the sole nitrogen source under fully aerobic conditions (*SI Appendix*, Fig. S9). *M. gorgona* MG08 shares this ability with the closely related *M. acidiphila* B2^T, and nonmethanotrophic members of the genus *Beijerinckia*, while *Methylocystis* and *Methylosinus*

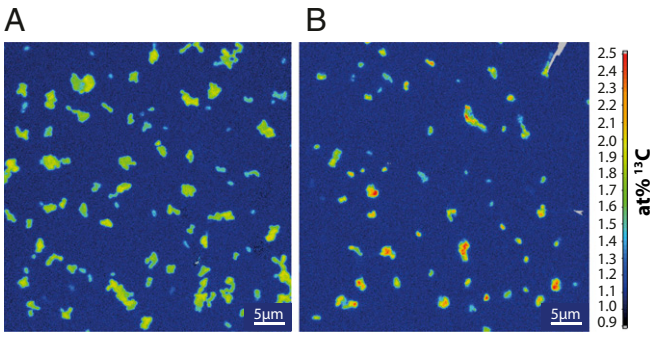

Fig. 7. Carbon fixation in *M. gorgona* MG08. NanoSIMS visualization of the ^{13}C isotope label incorporation in *M. gorgona* MG08 cells grown on polycarbonate filters in atmospheres containing 20 p.p.m.v. CH_4 and 1,000 p.p.m.v. CO_2. Two incubations are compared: $^{13}CH_4$ in combination with $^{12}CO_2$ (*A*) and $^{12}CH_4$ in combination with $^{13}CO_2$ (*B*). $^{13}C/(^{12}C + {}^{13}C)$ isotope fraction values, given in at%, are displayed on a false color scale ranging from 0.9 at% (dark blue) to 2.5 at% (red). Cells grown in isotopically unlabeled methane and carbon dioxide showed a ^{13}C content of 1.09 ± 0,01 at% (SD, $n = 60$).

species require a somewhat reduced oxygen tension and *Methylococcus capsulatus* (Bath) is highly sensitive to oxygen (39, 57, 58). Almost all tested nitrogen containing compounds including N_2, NO_3^-, and NH_4^+ acted as good nitrogen sources for *M. gorgona* MG08 (*SI Appendix*, Fig. S9), while histidine and glycine inhibited growth as shown previously for *M. capsulatus* (only histidine) (59), *Thiobacillus neapolitanus* (only histidine) (60), and methylotrophic bacteria (only glycine) (61).

No growth was observed in liquid batch culture controls provided with acetate, ethanol, formate, galactose, glucose, methanol, oxalate, pyruvate, sucrose, succinate, or urea without added CH_4 (*SI Appendix*, Fig. S10*A*). To evaluate potential concentration effects of methanol, we attempted growth on 5%, 0.5%, 0.01%, 0.005%, and 0.001% CH_3OH, but observed only minimal increases in the optical density of the cultures (*SI Appendix*, Fig. S10*B*). Considering that *M. gorgona* MG08 carries and expresses the genes for methanol oxidation, its inability to grow on methanol was surprising but it is in line with the observations that *M. aurea*, *M. acidiphila*, and *Methylocapsa palsarum* grow poorly on methanol (39, 62, 63). Interestingly, we observed a concentration-dependent growth inhibition of *M. gorgona* MG08 in the presence of methanol concentrations ≥0.01% when growing on CH_4 (20% CH_4 in headspace). Thus, toxicity alone could not explain its inability to use methanol. Perhaps methanol dehydrogenase, which requires oxidized cytochrome *c* for accepting electrons, thus depends on simultaneous CH_4 oxidation (Fig. 4) due to tightly coupled CH_4 and methanol oxidation reactions ocurring within a supercomplex. If so, the redox interactions would be different from intracytoplasmic membrane assemblies of pMMO and methanol dehydrogenase (MDH) in the methanol and CH_4 utilizing *M. capsulatus* (Bath) (64).

The incapability of *M. gorgona* MG08 to grow on acetate was also surprising, considering that it carries all of the genes required for aerobic metabolization of acetate, i.e., acetate-coA ligase, acetate kinase, phosphotransacetylase, and a complete TCA cycle. Similarly, *M. acidiphila* B2^T also possesses the full set of enzymes for acetate metabolism (65), but is unable to grow on acetate as a sole carbon source (39). Dedysh et al. (66) reported similar findings for the obligate methanotroph *Methyloferula stellata* AR4^T and suggested that the lack of ability to utilize acetate might be due to an absence of a specific acetate/glycolate transporter gene, *actP*, rather than the quantity of membrane transporter genes (67, 68). In support of this hypothesis, the *actP* gene encoding acetate permease is absent both in strain *M. gorgona* MG08 and *M. acidiphila* B2^T.

The cells of *M. gorgona* MG08 are Gram-negative, nonmotile coccoids, or thick rods that occur singly or in conglomerates. Cells are 0.6–0.8 μm wide and 0.8–1.5 μm long and show numerous hair-like structures (Fig. 1*B*). Growth on surfaces occurs by formation of microcolonies of a circular form. It reproduces by normal cell division and does not form rosettes. Cells contain a well-developed intracytoplasmic membrane system of type III arrangement, which appears as stacks of membrane vesicles packed in parallel on only one side of the cell membrane (Fig. 1*C*). This arrangement has been shown to be characteristic for members of the *Methylocapsa* genus (39, 62, 63). Inclusions resembling PHB granules were present (Fig. 1*C*) but did not exhibit the bipolar arrangement of refractile PHB granules characteristic of *M. aurea* KYG^T and members of the *Methylocella* genus. Optimal growth was observed between 15 °C and 27 °C, while some growth still occurred at the extremes tested, 7 °C and 37 °C (*SI Appendix*, Fig. S11*A*). The optimum growth temperature range was similar to but wider than *M. aurea* (25–30 °C), and higher/wider than that of *M. acidiphila* (20 °C) and *M. palsarum* (18–25 °C) (39, 62, 63). *M. gorgona* MG08 is thus far the only *Methylocapsa* strain capable of growth at 37 °C. The optimum pH for growth of *M. gorgona* MG08 was in the range of 6.5 to 7 (*SI Appendix*, Fig. S11*B*), considerably higher than for *M. acidiphila* (5.0–5.5), *M. aurea* (6.0–6.2), and *M. palsarum* (5.2–6.5), but in line with the frequent detection of USCα in neutral and slightly acidic soils (8, 16). NaCl was shown to inhibit growth at 0.5% (wt/vol) and above (*SI Appendix*, Fig. S11*C*), similarly to the three other *Methylocapsa* strains (39, 62, 63).

Conclusions

We have obtained a pure culture of an organism growing on ambient air containing an atmospheric methane concentration and named it *M. gorgona* MG08. *M. gorgona* MG08 utilizes CH_4 as a carbon and energy source and we have experimentally demonstrated that it can utilize at least three additional constituents of air: CO_2 as an additional carbon source, N_2 as a nitrogen source, and O_2 as terminal electron acceptor. Furthermore, it carries and expresses the genes necessary to exploit two additional atmospheric components, CO and H_2, as energy sources. Such metabolic flexibility may account for the enigmatic lifestyle of atmospheric CH_4 oxidizers and explain how they can grow on air alone. However, *M. gorgona* MG08 also grows efficiently at high CH_4 concentrations, but expresses only one pMMO, demonstrating that this enzyme is responsible for CH_4 oxidation at high and low concentrations. In line with this, *M. gorgona* MG08 has the highest specific affinity (a^0_s) for CH_4 of any known methane oxidizing bacterium, resulting from a high $V_{max(app)}$ despite a high $K_{m(app)}$. Furthermore, relatives within the genus *Methylocapsa* previously thought not to live on trace gases were shown to be able to grow on air as well, indicating that this ability is more widespread than previously believed. The isolation and characterization of a member of these recalcitrant organisms have direct implications for our understanding of the biological sink of atmospheric CH_4 and how atmospheric trace gases support life on our and possibly other planets.

Materials and Methods

Enrichment, Isolation, and Cultivation. The sampling site for *M. gorgona* MG08 was cover soil in a ditch in a retired subarctic landfill in northern Norway (69° 39′ N 18° 59′ E). Five grams of soil was added to 50 mL nitrate mineral salt medium (0.1× NMS) at pH 6.8 (DSMZ medium 921). Samples were shaken and streaked onto Whatman polycarbonate filters (Nucleopore Track-Etch membrane, pore size 0.2 μm). The filters were left floating on liquid 0.1× NMS in Petri dishes and incubated at room temperature (21–23 °C) in a chamber with ∼20% (vol/vol) CH_4 in the headspace. Colonies that appeared after incubation were purified by alternating between liquid, agar, and filter cultures. The pure culture of *M. gorgona* MG08 was maintained in liquid NMS medium. To verify liquid culture purity and absence of heterotrophic growth, the culture was checked by inoculating rich medium [tryptone, glucose, yeast extract, agar (TGYA)] with culture aliquots. This was done routinely in addition to microscopy. For cultivation in liquid, 10 mL culture was incubated in 125-mL serum bottles with air containing 20% CH_4 as headspace (vol/vol), without shaking. Serum bottles were closed with butyl rubber septa and crimp caps. For cultivation on plates, NMS agar plates were made with bacteriological agar type E (Biokar Diagnostics). Unless otherwise stated, all liquid and plate incubations were done at room temperature (21 °C) in the dark.

We observed a weak, but visible, growth of the culture on NMS agar plates after a 5-mo incubation on air. Based on this observation, a series of experiments was initiated. Initially, *M. gorgona* MG08 was inoculated in NMS medium without CH_4 addition in Erlenmeyer beakers, with parafilm lids, to which sterile distilled water was added every 2–4 wk to compensate for evaporation. Other incubations were done in serum bottles with 20 p.p.m.v. to 20% CH_4 in the headspace (vol/vol). In the cultures with less than 1,000 p.p.m.v. CH_4 in the headspace, there was no increase in optical density during the course of 8 mo of incubation. *M. gorgona* MG08 cells were nevertheless still alive after these long incubations, evidenced by rapid increase in optical density following their transfer to liquid medium with 20% CH_4 (vol/vol) in the headspace. As growth of *M. gorgona* MG08 on air could not be demonstrated by standard cultivation in liquid media, microcolony-growth experiments on polycarbonate filters floating on liquid NMS medium were performed.

A culture of *M. gorgona* MG08 was incubated for 2 mo in liquid NMS with 200 p.p.m.v. CH_4 in the headspace as start culture for microcolony growth on filters. The cell concentration in the suspension was determined by fluorescence microscopy after filtration on Anodisc filters (Whatman 6809-6022) and 1,000× SYBRgreen I (Molecular Probes S-7563) staining. For staining, filters were transferred (bacteria side up) on top of 200-μL droplets of 1,000× SYBRgreen and incubated for 10 min. In the next step, filters were washed twice by transferring them onto 1 mL milliQ water and then air dried. The whole procedure was performed at room temperature and in the dark. A fresh-made antifading solution consisting of 0.1% p-phenylenediamine dihydrochloride in 1:1 glycerol and PBS (pH 7.2) was used for mounting the filters on slides with coverslips.

A cell density of 20–50 cells per 50 × 50 μm filter area was selected for microcolony cultivation. A filtration manifold with 10 × 20 mL stainless steel chimneys (DHI LAB Products) was used for preparation of filters. Each well was washed with 70% ethanol and rinsed with sterile dH_2O before a GF/C filter (25 mm Whatman) was added as support filter. A polycarbonate filter (25 mm Nucleopore 110606) was then added before the chimney was placed on top. Even distributions of cells on the filters were obtained by pouring 12 mL NMS medium into the chimney before mixing in the cells and applying vacuum. The chimney walls were rinsed with 2 × 5 mL sterile water during suction. The polycarbonate filters were then transferred to Petri dishes with 20 mL liquid NMS medium and floated with the bacteria on the upper side. The dishes were either wrapped with parafilm and incubated in ambient air or stacked in 8.5-L jars (BD BBL GasPak 150) and incubated in air to which CH_4 was added to obtain 20, 50, or 1,000 p.p.m.v. CH_4 in the headspace. The filters were harvested after 17 d and transferred to freshly made 2% paraformaldehyde in 1× PBS for fixation in the refrigerator overnight.

Microcolony staining was performed following the procedure described above for the Anodisc filters. Stained cells were visualized by spinning disk confocal microscopy using an Axio Observer Z1 inverted microscope (Carl Zeiss Microscopy) equipped with a CSU-X1 scan head (Yokogawa) and a 100× NA1.4 plan-apochromat objective lens. SYBRgreen fluorescence was excited by the 488-nm laser line and collected through a 500- to 550-nm bandpass filter. Z stacks were captured with a Rolera EMC2 EM-CCD camera (QImaging) using ZEN ver. 2.3 (Carl Zeiss Microscopy), deconvolved in Huygens ver. 14.10 (SVI) using a theoretical point spread function, and finally exported as maximum intensity projections. An Axio Observer Z1 microscope with filter cube 38 was used for routine observations. Scanning electron microscopy (SEM) was performed at the Electron Microscope Laboratory, UiT The Arctic University of Norway. SEM samples were fixed and prepared as described previously (63) and scanned with a Carl Zeiss Zigma Field Emission scanning electron microscope.

Cultivation Experiments in Liquid Culture. All liquid culture experiments were conducted on 2-wk- and 4-wk-old batch cultures grown in sealed vials with 20% CH_4 (vol/vol). pH range was tested in NMS medium containing 0.1 M phosphate buffer ranging from pH 5 to pH 9 obtained by mixing 0.1 M solutions of KH_2PO_4 and K_2HPO_4 for 7 d. NaCl-dependent growth was determined over the range of 0.01–5.0% (wt/vol) for 24 d. Temperature tolerance was tested from 7 °C to 37 °C for 24 d. Methanol utilization was tested over a range of 0.001–5% (vol/vol). The following carbon sources

were tested at a concentration of 0.05% (wt/vol): acetate, ethanol, formate, galactose, glucose, methanol, oxalate, pyruvate, succinate, sucrose, and urea. Utilizable nitrogen sources were assessed by replacing KNO_3 in liquid NMS medium with 0.05% (wt/vol) L-alanine, L-arginine, L-asparagine, L-aspartate, L-cysteine, L-glutamate, glycine, L-histidine, L-isoleucine, NH_4Cl, yeast extract, or peptone. Growth on nitrogen sources was compared with growth in nitrogen-free NMS medium to assess N_2-fixation capability. Nitrogen fixation was further tested in nitrogen-free medium under microoxic [5% O_2 (vol/vol) with liquid comprising half volume] vs. fully oxic conditions and stationary vs. shaking conditions (150 rpm). Experiments were conducted on cells grown in liquid NMS medium with 20% (vol/vol) methane in the headspace. Growth was monitored for 30 d, unless otherwise stated, by optical density comparison with a respective control at 600 nm using a Spectramax 250 microplate spectrophotometer system (Molecular Devices).

CH_4 Oxidation in Atmospheric and Artificial Air and Inorganic Filter Controls. Five 170-mL bottles with floating polycarbonate filters were incubated on 35 mL 1/10 diluted NMS (diluted with phosphate buffer pH 6.8) under atmospheric air (135 mL 1 atm headspace, sealed with rubber stopper) for 120 d. An additional set of five bottles was incubated without filters as a negative control for CH_4 oxidation. All filters had ∼150–250 cells per 50 × 50 μm. For CH_4 measurements, 0.5 mL of headspace gas was sampled with a gastight gas chromatograph (GC) syringe (Hamilton). The contained gas was injected manually into a GC Thermo Fisher Scientific Trace 1310 with column TG-BOND Msieve 5A. Detection was achieved with a flame ionization detector (FID) with a detection limit of ∼0.5 ppm CH_4. Standards at 1.8 p.p.m.v. (air) and 10 p.p.m.v. CH_4 were checked at startup every day, and regularly during each batch of measurements. All calculations of actual concentrations accounted for the removal of gas for measurements. Growth tests were also performed on ultra-pure, carbon-free Anodisc inorganic filter membranes (25 mm, pore size 0.02 μm; Whatman) and polycarbonate filters (25 mm; Nucleopore 110606). All experiments were conducted using cells from the same batch of liquid culture (NMS), preincubated for 2 mo under a headspace atmosphere containing atmospheric air and 200 p.p.m.v. CH_4. Filters with cells were prepared as described above for microcolony cultivation. Diluted NMS was used to avoid previously experienced issues with crystal formation on filters due to high salt concentrations. No reductions in growth resulting from dilution were observed.

CH_4 Oxidation Experiment in Liquid Culture for Estimation of Kinetics Parameters. From log-phase batch cultures cultivated at 21 °C under 20% headspace CH_4 concentrations in liquid NMS medium, all cultures for the CH_4 oxidation experiments were prepared. Triplicate cultures with 21.6 mL of 5×10^7 cells per milliliter (culture diluted to the right density with phosphate buffer, pH 6.8) and one negative control with sterile NMS diluted with phosphate buffer (pH 6.8) were prepared for each of the following CH_4 concentrations: 823 p.p.m.v. headspace (1.26 μM dissolved), 0.23% (3.5 μM), 0.77% (11.8 μM), 2.2% (33 μM), 3.9% (59 μM), 5.1% (77.2 μM), and 6% (92.2 μM). All 28 samples were incubated for 8 h at 21 °C. CH_4 concentration was measured and optical density was measured at time (T) 0, 2.5 h, 5 h, and 8 h. For CH_4 measurements, headspace gas was sampled with a pressure-lock 1-mL gas syringe (VICI) with a side-port needle (0.020 × 0.012 × 2 inches; VICI). The pressure in the syringe was adjusted to ambient pressure, and the contained gas was injected into a gas chromatograph (SRI 8610C, FID configuration). At each time point, 340 μL of the culture was sampled in parallel. The optical density was determined by measurement using a Spectra Max 250 microplate reader, Molecular Devices at 410 nm (NMS diluted with phosphate buffer as blank). Cell densities were converted to cell numbers by separate standards for each culture, where the spectrophotometric density measurements of cell culture dilution series were associated to cell counts obtained using counting chambers. To account for the proportion of dissolved gases at 21 °C, masses of CH_4 were calculated from Henry's law, assuming an ideal state, knowing the ambient pressure, temperature, and headspace volume of the bottle at ambient pressure, liquid volume, mixing ratio of CH_4 and the temperature-dependent solubility constant. All calculations accounted for removal of gas and liquid for measurements. $V_{max(app)}$, $K_{m(app)}$, and associated SEs of their means were estimated by nonlinear regression using the R-package nlstools and its built-in functions "michaelis" and "nlsBoot" (69) with 10,000 bootstrap iterations. Specific affinities were calculated as shown previously.

Cultivation of *M. acidiphila* and *M. aurea* Under Atmospheric Air. Filters with *M. acidiphila*, *M. aurea*, and a control with *M. gorgona* MG08 were prepared as described for microcolony cultivation of *M. gorgona* MG08. In this experiment, all filters were incubated under atmospheric air on 1/10 NMS (diluted with phosphate buffer) with a pH of 5.8 (*M. acidiphila* and *M. aurea*) and pH 6.8 (*M. gorgona* MG08).

Morphological Observations. All morphological tests were conducted on 2-wk- and 4-wk-old batch cultures grown in liquid NMS in sealed vials with 20% CH_4 (vol/vol). Cell morphology and results of the Gram-stain reaction were determined by light microscopy. Lysis in 0.2% and 2% (wt/vol) SDS and lysis in 3% KOH was measured using an inoculum loop to assess colony viscosity (70). The presence of PHB inclusions was identified by visual inspection of transmission electron micrographs and confirmed by staining with Nitrile blue A (71). Exospore formation was assessed by heating cells at 80 °C for 20 min and observing colony formation on NMS agar after 2 wk of incubation with methane (72). Cyst formation was assayed by the method of Vela and Wyss (73) and by phase-contrast microscopy for stationary-phase liquid and plate cultures.

NanoSIMS. Microcolony cultivation with either $^{13}CH_4$ or $^{13}CO_2$ (in the presence of the corresponding unlabeled gas) was done at 20 p.p.m.v. CH_4 headspace concentration. Before use, the polycarbonate filters were coated with a gold-palladium (AuPd) alloy thin film (nominal thickness approximately 30 nm) in a low vacuum sputter coater utilizing argon as the working gas. The start culture consisted of a cell culture of *M. gorgona* MG08 grown in liquid NMS with a headspace atmosphere consisting of 200 p.p.m.v. CH_4 in ambient air. The cell density for NanoSIMS was five times higher than the density for microcolony cultivation. The cells were filtered onto the AuPd-coated filters in the way as described above. The filters were transferred to Petri dishes containing 20 mL liquid NMS medium pH 6.8 with the filters floating bacterial side up. Cultivation was done in 8.5 L jars to which gas volume was added by syringe. The filters were harvested at day 17 and fixed in the fridge overnight on freshly prepared 2% paraformaldehyde in 1× PBS. Using the vacuum filtration unit, filters were washed with 10 mL 1/2× PBS and then 10 mL milliQ. The filters were then left floating on milliQ water for 2× for 1 min before drying in darkness on glass slides shielded with plastic frames. For NanoSIMS analysis, 7 × 7 mm square sections were cut from the central area of the filters and attached to antimony-doped silicon wafer platelets (Active Business Company) with commercially available superglue (Loctite, Henkel). The samples were coated with an additional AuPd film (nominal thickness 30 nm) because some of the films deposited on the filters before the incubation provided insufficient electrical conductivity for charge compensation in the NanoSIMS measurement process.

NanoSIMS measurements were performed on a NanoSIMS NS50L instrument (Cameca). Data were acquired as multilayer image stacks by scanning a finely focused Cs^+ primary ion beam over areas between 45 × 45 and 50 × 50 μm^2 with a 512 × 512 pixel image resolution and approximately 80 nm physical resolution (probe size). The applied primary ion beam current and dwell time were 2.0 pA and 10 ms/(layer × pixel), respectively. The detectors of the multicollection assembly were positioned for parallel detection of $^{12}C^-$, $^{13}C^-$, $^{12}C_2^-$, $^{12}C^{13}C^-$, $^{12}C^{14}N^-$, $^{31}P^-$, and $^{32}S^-$ secondary ions. The mass spectrometer was tuned to achieve a mass resolving power (MRP) of >9,000 for detection of C^- and >10,000 for C_2^- secondary ions (MRP according to Cameca's definition). Information about topographical/morphological features within the samples was inferred from simultaneously recorded secondary electron intensity distribution images.

Analyses were performed either on entire cells (long-term acquisition runs) or by sampling partial cell volumes, in both cases accessed by presputtering with a slightly defocused, high-intensity primary ion beam. Data comparison was performed on image data acquired from regions close to the center of the cells which were reached after irradiation of paraformaldehyde-fixed *M. gorgona* MG08 cells with 16 keV Cs^+ primary ions at a fluence (dose density) of 3×10^{16} ions/cm^2.

Image data were evaluated using the WinImage software package provided by Cameca (version 2.0.8). Before stack accumulation, the individual images were aligned to compensate for positional variations arising from primary ion beam and/or sample stage drift. Secondary ion signal intensities were dead time corrected on a per-pixel basis. Carbon isotope composition images were generated by calculation of per-pixel $^{13}C/(^{12}C + {}^{13}C)$ isotope fraction values, given in atom percent (at%), from the C^- and C_2^- secondary ion signal intensities via $^{13}C^-/(^{12}C^- + {}^{13}C^-)$ and $^{13}C^{12}C^-/(2 \times {}^{12}C_2^- + {}^{13}C^{12}C^-)$, respectively. All carbon isotope composition data given in the paper were inferred from C_2^- signal intensities owing to the superior counting statistics of this secondary ion species. We did not observe any significant differences between isotope fraction values inferred from C_2^- or C^- signal intensities.

Concentrations and carbon isotope ratio of CO_2 (in thousandth relative to the Vienna Pee Dee Belemnite standard) was determined via a Gas-Bench II interfaced to continuous-flow gas isotope ratio mass spectrometry (Delta V Advantage, Thermo Fisher Scientific).

Genome Sequencing and Annotation. The standard protocol of DOE Joint Genome Institute (JGI; 1ofdmq2n8tc36m6i46scovo2e-wpengine.netdna-ssl.com/wp-content/uploads/2014/02/JGI-Bacterial-DNA-isolation-CTAB-Protocol-2012.pdf), was used for DNA isolation from cells grown in liquid culture. Whole-genome sequencing was performed on a Pacific Biosciences RS II instrument using P4-C2 chemistry. Two single molecule real-time sequencing (SMRT) cells were used for sequencing at Norwegian Sequencing Centre Oslo, Norway (https://www.sequencing.uio.no). Reads were assembled using HGAP v3 (SMRT Analysis Software v2.2.0, Pacific Biosciences). Minimus2 software of the Amos package was used to circularize contigs, which were confirmed by dotplot to contain the same sequence at the beginning and end of the contig. RS_Resequencing.1 software (SMRT Analysis version v2.2.0) was used to map reads back to assembled and circularized sequence to correct the sequence after circularization. The complete genome sequence of this strain was determined from 94,080 long reads (Pacific Biosciences) which assembled 94 into a single circular chromosome with a size of 3,326,440 bp and a GC content of 58.94%, a per-base coverage of 121 and consensus accuracy of 99.9998%. All reads mapped to the genome, indicating that no contaminating organisms were present in the culture. Genome annotation was carried out using tools of the MicroScope platform (74). The metabolism of *M. gorgona* MG08 was reconstructed manually using the MicroScope annotation, supplemented with protein Blast searches (75), multiple gene sequence alignments using Clustal W (76), and phylogenetic calculations using Mega 7 (77) as described in the figure legends of the respective phylogenetic trees. Alignment visualization of 16S rRNA genes was created using JalView (78). For functional classification, protein sequences encoding CO dehydrogenase, hydrogenase, and RuBisCO were aligned with reference sequences reported previously (49). A phylogenomic tree was calculated in PhyloBayes (79). The input alignment of 34 concatenated marker genes was generated using CheckM (80) and the model and number of rate categories was identified using ModelFinder (81). gANI (82) and average AAI values (83) were calculated using annotated genes supplemented with additional gene calls predicted by Prodigal (83). gANI was calculated using Microbial Species Identifier (MiSI) (82). For AAI, bidirectional best hits were identified using blastp, requiring that query genes aligned over at least 70% of their length to target genes (in each unidirectional blastp search). Query gene length was used to calculate a weighted average proportional (percentage) identity over all best hit pairs and the calculations were repeated using each genome as query and target. The full-length 16S rRNA sequence from *M. gorgona* MG08 was used to screen 183,153 Short Read Archive (SRA) datasets with IMNGS (84) using a minimum threshold of 97% identity and a minimum size of 200 nucleotides. Short reads identified with IMNGS were aligned to the 16S rRNA alignment used to produce *SI Appendix*, Fig. S1 with SINA (85). Reads were then placed into the tree shown in *SI Appendix*, Fig. S1 using the evolutionary placement algorithm (EPA) in RAxML (86). Only reads that were assigned to the branch leading to *M. gorgona* MG08 were considered "positive" for *M. gorgona* MG08. Metadata for read sets were downloaded using efetch from NCBI E-utilities and latitude/longitude coordinates were extracted using the ElementTree XML API in Python. Coordinates associated with *M. gorgona*-positive read sets were plotted using the mapproj library in R, with a Mollweide projection. Hydrogenases were classified using the web tool HydDB (87). Heme-copper cytochrome *c* oxidases were classified using the web tool HCO (88). Homologs to genes encoding the central metabolism of *M. gorgona* MG08 were identified in related species and MAGs using BLAST (75), Orthofinder (89), and manual curation of results.

Protein Extraction and Mass Spectrometry. Proteomics was conducted on a 2-wk-old batch culture grown in sealed vials with 20% CH_4 (vol/vol). Proteins were extracted from pelleted cells using SDS buffer (0.1 M Tris·HCl, pH 7, 1.25% wt/vol SDS, 20 mM dithiotreitol) and ultrasonication for 3 min (80% power, 0.8 amplitude) as described (90). Protein pellets were dissolved in 20 μL SDS sample buffer (2% SDS, 2 mM beta-mercaptoethanol, 4% glycerol, 40 mM Tris·HCl pH 6.8, 0.01% bromophenolblue), heated to 90 °C for 5 min and separated on a 1D SDS gel. After a short run (10 min) the gel was stained with Coomassie G-250 staining (Merck). The stained gel band was cut, destained, dehydrated, and incubated with trypsin (Promega) overnight at 37 °C. The resulting peptides were desalted using C_{18} ZipTip column (Merck Millipore) and subsequently dissolved in 0.1% formic acid before liquid chromatography mass spectrometry analysis (nanoLC-MS/MS). Peptide lysates (5 μL) were first loaded for 5 min on the precolumn (μ-precolumn, Acclaim PepMap, 75-μm inner diameter, 2 cm, C18; Thermo Fisher Scientific), at 4% mobile phase B (80% acetonitrile in nanopure water with 0.08% formic acid) and 96% mobile phase A (nanopure water with 0.1% formic acid), and then eluted from the analytical column (PepMap Acclaim C18 LC Column, 25 cm, 3 μm particle size; Thermo Fisher Scientific) over a 150-min linear gradient of mobile phase B (4–55% B). Mass spectrometry was performed on a Q Exactive HF mass spectrometer (Thermo Fisher Scientific) with a TriVersa NanoMate (Advion, Ltd.) source in LC-chip coupling mode as described (91).

Proteome Discoverer (v1.4.0.288, Thermo Fisher Scientific) was used for protein identification and the MS/MS spectra acquired were searched with Sequest HT against the complete genome sequence for strain *M. gorgona* MG08. Enzyme specificity was selected as trypsin with up to two missed cleavages allowed, using 10-ppm peptide ion tolerance and 0.05-Da MS/MS tolerances. Oxidation at methionines as the variable modifications and carbamidomethylation at cysteines as the static modification were selected. Only peptides with a false discovery rate (FDR) <1% calculated by Percolator (92) were considered as identified.

ACKNOWLEDGMENTS. We thank Matteus Lindgren for help with gas chromatography measurements, Holger Daims for comments on the manuscript, Nicholas Tyler for language corrections, and the US–Norway Fulbright Foundation for a scholarship (to S.L.R.). C.H., A.S., and M.W. were supported by the European Research Council (ERC) Advanced Grant Project NITRICARE 294343 (to M.W.). A.T.T. was supported by the Research Council of Norway FRIPRO Mobility Grant Project Time and Energy 251027/RU, cofunded by ERC under Marie Curie Grant 608695, and Tromsø Research Foundation starting grant project Cells in the Cold 17_SG_ATT. S.N.D. and M.M.S. were supported by the collaborative project between the Russian Fund of Basic Research (Grant 14-04-93082) and the Research Council of Norway (Grant 233645/H30).

1. Prather MJ, Holmes CD (2017) Overexplaining or underexplaining methane's role in climate change. *Proc Natl Acad Sci USA* 114:5324–5326.
2. IPCC (2013) *Climate Change 2013–The Physical Science Basis, Contribution of Working Group I to the Fifth Assessment Report of the IPCC* (Cambridge Univ Press, Cambridge, UK).
3. Dlugokencky EJ, Nisbet EG, Fisher R, Lowry D (2011) Global atmospheric methane: Budget, changes and dangers. *Philos Trans A Math Phys Eng Sci* 369:2058–2072.
4. Kirschke S, et al. (2013) Three decades of global methane sources and sinks. *Nat Geosci* 6:813–823.
5. Conrad R (2009) The global methane cycle: Recent advances in understanding the microbial processes involved. *Environ Microbiol Rep* 1:285–292.
6. Dunfield PF (2007) The soil methane sink. *Greenhouse Gas Sinks*, eds Reay DS, Hewitt CN, Smith KA, Grace J (CABI, Wallingford, UK), pp 152–170.
7. Shallcross DE, Butenhoff CL (2007) The atmospheric methane sink. *Greenhouse Gas Sinks*, eds Reay DS, Hewitt CN, Smith KA, Grace J (CABI, Wallingford, UK), pp 171–184.
8. Knief C (2015) Diversity and habitat preferences of cultivated and uncultivated aerobic methanotrophic bacteria evaluated based on pmoA as molecular marker. *Front Microb,* 6:1346.
9. Hanson RS, Hanson TE (1996) Methanotrophic bacteria. *Microbiol Rev* 60:439–471.
10. Trotsenko YA, Murrell JC (2008) Metabolic aspects of aerobic obligate methanotrophy. *Adv Appl Microbiol* 63:183–229.
11. Sohngen NL (1906) Ueber Bakterien welche Methan als Kohlenstoffnahrung und Energiequelle gebrauchen. *Zentr Bakteriol Abt II* 15:513–517.
12. Bender M, Conrad R (1992) Kinetics of CH_4 oxidation in oxic soils exposed to ambient air or high CH_4 mixing ratios. *FEMS Microbiol Ecol* 10:261–269.
13. Whalen SC, Reeburgh WS (1990) Consumption of atmospheric methane by tundra soils. *Nature* 346:160–162.
14. Whalen SC, Reeburgh WS, Sandbeck KA (1990) Rapid methane oxidation in a landfill cover soil. *Appl Environ Microbiol* 56:3405–3411.
15. Yavitt JB, Downey DM, Lang GE, Sexston AJ (1990) Methane consumption in two temperate forest soils. *Biogeochemistry* 9:9–52.
16. Knief C, Lipski A, Dunfield PF (2003) Diversity and activity of methanotrophic bacteria in different upland soils. *Appl Environ Microbiol* 69:6703–6714.
17. Roslev P, Iversen N (1999) Radioactive fingerprinting of microorganisms that oxidize atmospheric methane in different soils. *Appl Environ Microbiol* 65:4064–4070.
18. Holmes AJ, et al. (1999) Characterization of methanotrophic bacterial populations in soils showing atmospheric methane uptake. *Appl Environ Microbiol* 65:3312–3318.
19. Baani M, Liesack W (2008) Two isozymes of particulate methane monooxygenase with different methane oxidation kinetics are found in *Methylocystis* sp. strain SC2. *Proc Natl Acad Sci USA* 105:10203–10208.
20. Dunfield PF, et al. (2002) Isolation of a *Methylocystis* strain containing a novel pmoA-like gene. *FEMS Microbiol Ecol* 41:17–26.
21. Kravchenko IK, Kizilova AK, Bykova SA, Men'ko EV, Gal'chenko VF (2010) Molecular analysis of high-affinity methane-oxidizing enrichment cultures isolated from a forest biocenosis and agrocenoses. *Microbiol* 79:106–114.
22. Cai Y, Zheng Y, Bodelier PL, Conrad R, Jia Z (2016) Conventional methanotrophs are responsible for atmospheric methane oxidation in paddy soils. *Nat Commun* 7:11728.
23. Knief C, Dunfield PF (2005) Response and adaptation of different methanotrophic bacteria to low methane mixing ratios. *Environ Microbiol* 7:1307–1317.

24. Degelmann DM, Borken W, Drake HL, Kolb S (2010) Different atmospheric methane-oxidizing communities in European beech and Norway spruce soils. *Appl Environ Microbiol* 76:3228–3235.
25. Pratscher J, Vollmers J, Wiegand S, Dumont MG, Kaster A-K (2018) Unravelling the identity, metabolic potential, and global biogeography of the atmospheric methane-oxidising upland soil cluster α. *Environ Microbiol* 20:1016–1029.
26. Kolb S, Knief C, Dunfield PF, Conrad R (2005) Abundance and activity of uncultured methanotrophic bacteria involved in the consumption of atmospheric methane in two forest soils. *Environ Microbiol* 7:1150–1161.
27. Shrestha PM, Kammann C, Lenhart K, Dam B, Liesack W (2012) Linking activity, composition and seasonal dynamics of atmospheric methane oxidizers in a meadow soil. *ISME J* 6:1115–1126.
28. Martineau C, et al. (2014) Atmospheric methane oxidizers are present and active in Canadian high Arctic soils. *FEMS Microbiol Ecol* 89:257–269.
29. Ricke P, et al. (2005) First genome data from uncultured upland soil cluster alpha methanotrophs provide further evidence for a close phylogenetic relationship to Methylocapsa acidiphila B2 and for high-affinity methanotrophy involving particulate methane monooxygenase. *Appl Environ Microbiol* 71:7472–7482.
30. Edwards CR, et al. (2017) Draft genome sequence of uncultured upland soil cluster *Gammaproteobacteria* gives molecular insights into high-affinity methanotrophy. *Genome Announc* 5:e00047-17.
31. Singleton CM, et al. (2018) Methanotrophy across a natural permafrost thaw environment. *ISME J* 12:2544–2558.
32. Horz HP, Rich V, Avrahami S, Bohannan BJ (2005) Methane-oxidizing bacteria in a California upland grassland soil: Diversity and response to simulated global change. *Appl Environ Microbiol* 71:2642–2652.
33. Semrau JD, et al. (2013) Methanobactin and MmoD work in concert to act as the 'copper-switch' in methanotrophs. *Environ Microbiol* 15:3077–3086.
34. Jwanoswki K, et al. (2017) The *Legionella pneumophila* GIG operon responds to gold and copper in planktonic and biofilm cultures. *PLoS One* 12:e0174245.
35. Marx CJ, et al. (2012) Complete genome sequences of six strains of the genus *Methylobacterium*. *J Bacteriol* 194:4746–4748.
36. Vu HN, et al. (2016) Lanthanide-dependent regulation of methanol oxidation systems in *Methylobacterium extorquens* AM1 and their contribution to methanol growth. *J Bacteriol* 198:1250–1259.
37. Kallen RG, Jencks WP (1966) The mechanism of the condensation of formaldehyde with tetrahydrofolic acid. *J Biol Chem* 241:5851–5863.
38. Marx CJ, Chistoserdova L, Lidstrom ME (2003) Formaldehyde-detoxifying role of the tetrahydromethanopterin-linked pathway in *Methylobacterium extorquens* AM1. *J Bacteriol* 185:7160–7168.
39. Dedysh SN, et al. (2002) *Methylocapsa acidiphila* gen. nov., sp. nov., a novel methane-oxidizing and dinitrogen-fixing acidophilic bacterium from *Sphagnum* bog. *Int J Syst Evol Microbiol* 52:251–261.
40. Miroshnikov KK, et al. (2017) Draft genome sequence of *Methylocapsa palsarum* NE2^T, an obligate methanotroph from subarctic soil. *Genome Announc* 5:e00504-17.
41. Rasigraf O, Kool DM, Jetten MSM, Sinninghe Damsté JS, Ettwig KF (2014) Autotrophic carbon dioxide fixation via the Calvin-Benson-Bassham cycle by the denitrifying methanotroph "*Candidatus* Methylomirabilis oxyfera". *Appl Environ Microbiol* 80:2451–2460.
42. Vorobev AV, et al. (2011) *Methyloferula stellata* gen. nov., sp. nov., an acidophilic, obligately methanotrophic bacterium that possesses only a soluble methane monooxygenase. *Int J Syst Evol Microbiol* 61:2456–2463.
43. Chen Y, et al. (2010) Complete genome sequence of the aerobic facultative methanotroph *Methylocella silvestris* BL2. *J Bacteriol* 192:3840–3841.
44. Khadem AF, et al. (2011) Autotrophic methanotrophy in verrucomicrobia: *Methylacidiphilum fumariolicum* SolV uses the Calvin-Benson-Bassham cycle for carbon dioxide fixation. *J Bacteriol* 193:4438–4446.
45. Tabita FR, Hanson TE, Satagopan S, Witte BH, Kreel NE (2008) Phylogenetic and evolutionary relationships of RubisCO and the RubisCO-like proteins and the functional lessons provided by diverse molecular forms. *Philos Trans R Soc Lond B Biol Sci* 363:2629–2640.
46. Figueroa IA, et al. (2018) Metagenomics-guided analysis of microbial chemolithoautotrophic phosphite oxidation yields evidence of a seventh natural CO_2 fixation pathway. *Proc Natl Acad Sci USA* 115:E92–E101.
47. Hartmann T, Leimkühler S (2013) The oxygen-tolerant and NAD+-dependent formate dehydrogenase from *Rhodobacter capsulatus* is able to catalyze the reduction of CO_2 to formate. *FEBS J* 280:6083–6096.
48. Klotz MG, Stein LY (2008) Nitrifier genomics and evolution of the nitrogen cycle. *FEMS Microbiol Lett* 278:146–156.
49. Ji M, et al. (2017) Atmospheric trace gases support primary production in Antarctic desert surface soil. *Nature* 552:400–403.
50. Greening C, Berney M, Hards K, Cook GM, Conrad R (2014) A soil actinobacterium scavenges atmospheric H_2 using two membrane-associated, oxygen-dependent [NiFe] hydrogenases. *Proc Natl Acad Sci USA* 111:4257–4261.
51. Ratcliff WC, Kadam SV, Denison RF (2008) Poly-3-hydroxybutyrate (PHB) supports survival and reproduction in starving rhizobia. *FEMS Microbiol Ecol* 65:391–399.
52. Pieja AJ, Sundstrom ER, Criddle CS (2011) Poly-3-hydroxybutyrate metabolism in the type II methanotroph *Methylocystis parvus* OBBP. *Appl Environ Microbiol* 77:6012–6019.
53. Belly RT, Lauff JJ, Goodhue CT (1975) Degradation of ethylenediaminetetraacetic acid by mictobial populations from an aerated lagoon. *Appl Microbiol* 29:787–794.
54. Honeycutt JA, Nguyen JQT, Kentner AC, Brenhouse HC (2017) Effects of water bottle materials and filtration on Bisphenol A content in laboratory animal drinking water. *J Am Assoc Lab Anim Sci* 56:269–272.
55. Vijayalakshmi V, et al. (2018) Bio-degradation of Bisphenol A by *Pseudomonas aeruginosa* PAb1 isolated from effluent of thermal paper industry: Kinetic modeling and process optimization. *J Radiat Res Appl Sci* 11:56–65.
56. Dunfield PF, Conrad R (2000) Starvation alters the apparent half-saturation constant for methane in the type II methanotroph *Methylocystis* strain LR1. *Appl Environ Microbiol* 66:4136–4138.
57. Dedysh SN, Ricke P, Liesack W, Nif H (2004) NifH and NifD phylogenies: An evolutionary basis for understanding nitrogen fixation capabilities of methanotrophic bacteria. *Microbiology* 150:1301–1313.
58. Murrell JC, Dalton H (1983) Nitrogen fixation in obligate methanotrophs. *J Gen Microbiol* 129:3481–3486.
59. Eccleston M, Kelly DP (1972) Assimilation and toxicity of exogenous amino acids in the methane-oxidizing bacterium *Methylococcus capsulatus*. *J Gen Microbiol* 71:541–554.
60. Johnson CL, Vishniac W (1970) Growth inhibition in *Thiobacillus neapolitanus* by histidine, methionine, phenylalanine, and threonine. *J Bacteriol* 104:1145–1150.
61. Ratomahenina R, Galzy P (1981) Mutation modifying the serine pathway in methylotrophic bacteria. *Folia Microbiol (Praha)* 26:179–183.
62. Dunfield PF, Belova SE, Vorob'ev AV, Cornish SL, Dedysh SN (2010) Methylocapsa aurea sp. nov., a facultative methanotroph possessing a particulate methane monooxygenase, and emended description of the genus Methylocapsa. *Int J Syst Evol Microbiol* 60:2659–2664.
63. Dedysh SN, et al. (2015) *Methylocapsa palsarum* sp. nov., a methanotroph isolated from a subArctic discontinuous permafrost ecosystem. *Int J Syst Evol Microbiol* 65:3618–3624.
64. Culpepper MA, Rosenzweig AC (2014) Structure and protein-protein interactions of methanol dehydrogenase from Methylococcus capsulatus (Bath). *Biochemistry* 53:6211–6219.
65. Tamas I, Smirnova AV, He Z, Dunfield PF (2014) The (d)evolution of methanotrophy in the Beijerinckiaceae–A comparative genomics analysis. *ISME J* 8:369–382.
66. Dedysh SN, et al. (2015) Draft genome sequence of Methyloferula stellata AR4, an obligate methanotroph possessing only a soluble methane monooxygenase. *Genome Announc* 3:e01555-14.
67. Chain P, et al. (2003) Complete genome sequence of the ammonia-oxidizing bacterium and obligate chemolithoautotroph Nitrosomonas europaea. *J Bacteriol* 185:2759–2773.
68. Ward N, et al. (2004) Genomic insights into methanotrophy: The complete genome sequence of Methylococcus capsulatus (Bath). *PLoS Biol* 2:e303.
69. Baty F, et al. (2015) A toolbox for nonlinear regression in R: The package nlstools. *J Stat Software* 66:1–21.
70. Jones DM (1981) Manual of methods for general bacteriology. *J Clin Pathol* 34:1069.
71. Ostle AG, Holt JG (1982) Nile blue A as a fluorescent stain for poly-beta-hydroxybutyrate. *Appl Environ Microbiol* 44:238–241.
72. Bowman JP, Sly LI, Nichols PD, Hayward AC (1993) Revised taxonomy of the methanotrophs: Description of Methylobacter gen. Nov., emendation of Methylococcus, validation of Methylosinus and Methylocystis species, and a proposal that the family Methylococcaceae includes only the group I methanotrophs. *Int J Syst Evol Microbiol* 43:735–753.
73. Vela GR, Wyss O (1964) Improved stain for visualization of Azotobacter encystment. *J Bacteriol* 87:476–477.
74. Vallenet D, et al. (2013) MicroScope–An integrated microbial resource for the curation and comparative analysis of genomic and metabolic data. *Nucleic Acids Res* 41:D636–D647.
75. Altschul SF, et al. (1997) Gapped BLAST and PSI-BLAST: A new generation of protein database search programs. *Nucleic Acids Res* 25:3389–3402.
76. Larkin MA, et al. (2007) Clustal W and clustal X version 2.0. *Bioinformatics* 23:2947–2948.
77. Kumar S, Stecher G, Tamura K (2016) MEGA7: Molecular Evolutionary Genetics Analysis version 7.0 for bigger datasets. *Mol Biol Evol* 33:1870–1874.
78. Waterhouse AM, Procter JB, Martin DM, Clamp M, Barton GJ (2009) Jalview version 2–A multiple sequence alignment editor and analysis workbench. *Bioinformatics* 25:1189–1191.
79. Lartillot N, Lepage T, Blanquart S (2009) PhyloBayes 3: A Bayesian software package for phylogenetic reconstruction and molecular dating. *Bioinformatics* 25:2286–2288.
80. Parks DH, Imelfort M, Skennerton CT, Hugenholtz P, Tyson GW (2015) CheckM: Assessing the quality of microbial genomes recovered from isolates, single cells, and metagenomes. *Genome Res* 25:1043–1055.
81. Kalyaanamoorthy S, Minh BQ, Wong TKF, von Haeseler A, Jermiin LS (2017) ModelFinder: Fast model selection for accurate phylogenetic estimates. *Nat Methods* 14:587–589.
82. Varghese NJ, et al. (2015) Microbial species delineation using whole genome sequences. *Nucleic Acids Res* 43:6761–6771.
83. Hyatt D, et al. (2010) Prodigal: Prokaryotic gene recognition and translation initiation site identification. *BMC Bioinformatics* 11:119.
84. Lagkouvardos I, et al. (2016) IMNGS: A comprehensive open resource of processed 16S rRNA microbial profiles for ecology and diversity studies. *Sci Rep* 6:33721.
85. Pruesse E, Peplies J, Glöckner FO (2012) SINA: Accurate high-throughput multiple sequence alignment of ribosomal RNA genes. *Bioinformatics* 28:1823–1829.
86. Berger SA, Krompass D, Stamatakis A (2011) Performance, accuracy, and Web server for evolutionary placement of short sequence reads under maximum likelihood. *Syst Biol* 60:291–302.
87. Søndergaard D, Pedersen CNS, Greening C, Hyd DB (2016) HydDB: A web tool for hydrogenase classification and analysis. *Sci Rep* 6:34212.
88. Sousa FL, Alves RJ, Pereira-Leal JB, Teixeira M, Pereira MM (2011) A bioinformatics classifier and database for heme-copper oxygen reductases. *PLoS One* 6:e19117.
89. Emms DM, Kelly S (2015) OrthoFinder: Solving fundamental biases in whole genome comparisons dramatically improves orthogroup inference accuracy. *Genome Biol* 16:157.
90. Türkowsky D, et al. (2018) A retentive memory of tetrachloroethene respiration in Sulfurospirillum halorespirans–Involved proteins and a possible link to acetylation of a two-component regulatory system. *J Proteomics* 181:36–46.
91. Starke R, et al. (2017) Candidate Brocadiales dominates C, N and S cycling in anoxic groundwater of a pristine limestone-fracture aquifer. *J Proteomics* 152:153–160.
92. Käll L, Canterbury JD, Weston J, Noble WS, MacCoss MJ (2007) Semi-supervised learning for peptide identification from shotgun proteomics datasets. *Nat Methods* 4:923–925.